Journal of the Technical University of Gabrovo

https://mc04.manuscriptcentral.com/jtug

INFLUENCE OF DIAMOND BURNISHING GOVERNING FACTORS ON THE SURFACE MICROHARDNESS OF AUSTENITIC STAINLESS STEELS

Mariana Ichkova*

Technical University of Gabrovo, 5300 Gabrovo, Bulgaria

ARTICLE INFO

Article history:
Received 10 May 2025
Accepted 24 June 2025

Keywords:
austenitic stainless steel, diamond burnishing, surface integrity, surface microhardness

http://doi.org/10.62853/WRDV8518

ABSTRACT

Diamond burnishing (DB) is an effective finishing that dramatically improves the performance of metal components due to the favorable combination of surface integrity characteristics. A comprehensive study of the effects of DB governing factors of AISI 304 steel specimens on the microhardness was conducted using an optimal second-order composition plan, ANOVA and regression analysis. Mathematical model of the surface microhardness depending on the burnishing force, feed rate and burnishing velocity was obtained. Based on the results obtained, it was found that the combination of high burnishing force, minimum feed rate and minimum burnishing velocity maximizes the surface microhardness.

1. INTRODUCTION

Chromium-nickel austenitic steels have superior general corrosion resistance, good machinability by cutting and plastic deformation, good weldability, and can be used from cryogenic to elevated temperatures, which is why they are widely used in many industries. A disadvantage of these steels under normal operating conditions is their insufficient hardness and strength. These properties can be improved by volume cold working [1, 2] or by modifying the surface layers (SL). The first approach requires a significant energy resource and is limited to blanks and details of sheet material. SL modification is achieved by low-temperature nitriding and/or carburizing to form the S-phase [3, 4], surface cold working [5, 6] or a combination of both [7, 8].

The formation of the S-phase is a valuable means of improving the hardness, fatigue strength, tribological properties and corrosion resistance of austenitic stainless steels. However, this process is time-consuming and expensive, due to its duration (typically 20-30 hours) and the requirement of special and expensive equipment. In addition, the S-phase is a metastable phase due to its tendency to transform when exposed to high temperatures. The maximum operating temperature is believed to be around 200°C [3].

An effective approach to modify SL is static surface cold working (SCW) [9]. In static SCW, a hard and smooth deforming element is pressed with a constant static force against the machined surface and performs relative movement with respect to it. Thus, the surface layer is plastically deformed at a temperature lower than the recrystallization temperature of the machined material. As a result, the roughness is drastically reduced, the surface microhardness is significantly increased, useful residual compressive stresses are introduced into the surface and nearby subsurface layers, and the microstructure in these layers is modified in the direction of grain refinement and orientation [10]. When the tangential contact between the deforming element and the machined surface is sliding friction, the static SCW is known as slide burnishing (SB) [11, 12]. SB can be implemented with a non-diamond [13, 14] or diamond [15] deforming element. In the latter case, SB is called slide diamond burnishing or diamond burnishing (DB). DB was introduced in 1962 by General Electric to improve the surface integrity (SI) of metal components. DB is a simple and effective finishing and its main advantage over roller burnishing [16] is the significantly simpler equipment with which DB is realized. The experimental comparison between DB and deep rolling process performed in [17] showed the advantage of DB in terms of SI and fatigue strength behaviour.

Over the past six decades, DB has established itself as an effective finisher for structural [18], tool [19] and stainless [20, 21] steels, high-strength titanium [22] and aluminum [23, 24] alloys, and bronze alloys [25-27].

Comprehensive studies on the effects of DB process on SI and the operational behavior in terms of fatigue, wear and corrosion resistance of specimens made of chromium-nickel austenitic steels were conducted in [8-10, 20, 21, 28-31]. However, only a small part of them contains information on the influence of the governing factors of DB process on the surface microhardness. In [9], based on a planned experiment, a microhardness model was established in which the variables were burnishing force and number of passes. The material was AISI 304 steel with a hardness of 245 HB. These authors found that with

* Corresponding author. E-mail: ichkova@tugab.bg

increasing burnishing force, the surface microhardness increases with a decreasing rate. With increasing number of passes to 3, the microhardness increases, then decreases. In [20], the influence of all governing factors of DB process on the surface microhardness of AISI 304 steel using one-factor-at-a-time technique was studied. Varga and Ferencsik [28] investigated the influence of burnishing force, feed rate and burnishing velocity on the surface microhardness of diamond burnished 304 steel specimens. The diamond insert radius and the material hardness were 3.5 mm and 215 HB respectively. However, these authors used a linear model of microhardness, but the effects related to plasticity are nonlinear.

Based on the review conducted, it can be concluded that there is a lack of systematized information on the influence of the governing factors of DB process on surface microhardness of diamond burnished chromium-nickel austenitic steels. Thus, the main objective of this study is to fill this gap.

2. MATERIALS AND METHODS

2.1. Material used

In this study, AISI 304 chromium-nickel austenitic stainless steel was selected, as this grade is the most commonly used in engineering practice. The material was obtained as hot-rolled bars with diameters of 16 mm and was used in as-received state. The chemical composition was established using optical emission spectrometer. Tensile tests at room temperature were carried out via Zwick/Roell Vibrophore 100 testing machine. The working sections of the tensile test specimens have a gauge diameter of 6 mm and a gauge length of 30 mm. The material hardness was measured via a VEB-WPM tester using a spherical-ended indenter having a diameter of 2.5 mm, loading of 63 kg, and holding time of 10 s.

2.2. DB implementation

DB (Fig. 1) was implemented on Index Traub CNC lathe using spherical-ended polycrystalline diamond insert with radius of 2 mm and conventional flood lubrication (Vasco 6000).

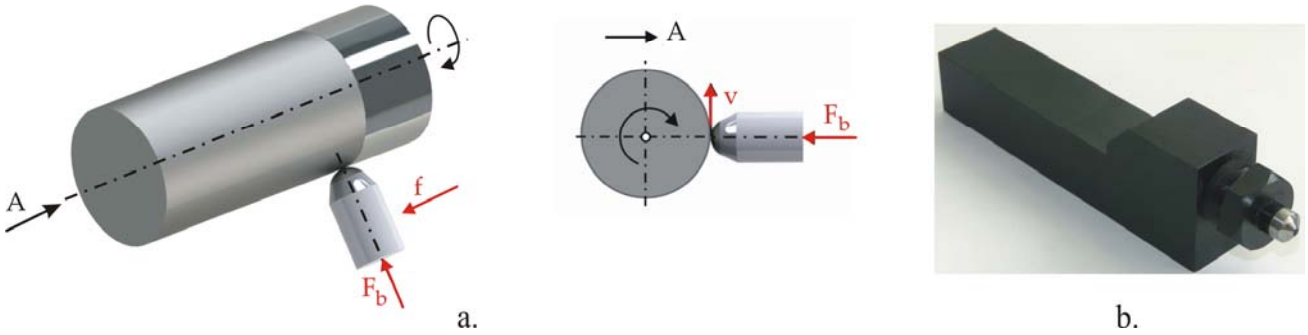

Fig. 1. DB implementation: a. kinematics and governing factors; b. DB device

The burnishing devices (Fig. 1b) provide elastic normal contact between the deforming element and the treated surface. Turning as premachining and DB were carried out on CNC lathe in one clamping process to minimize the concentric run-out in DB. VCMT 160404 – F3P carbide cutting insert (main back angle $\alpha_0 = 7^o$; radius at tool tip 0.4 mm) was used for the previous turning. SVJCR 2525M-16 holder with main and auxiliary setting angles $\chi_c = 93^o$ and $\chi_c' = 52^o$, respectively, was used. The cutting insert and the holder are manufactured by ISCAR Bulgaria.

2.3. Surface microhardness measurement

ZHVμ Zwick/Roell micro-hardness tester (Ulm, Germany) was used to establish the surface microhardnes. The loading and holding time were 0.05 kgf and 10 s, respectively. The final surface microhardness value was the center of clustering of ten measurements.

3. RESULTS AND DISCUSSION

3.1. Material identification

Table 1 shows the chemical composition of the used AISI 304 stainless steel. The remaining chemical elements (0.203 wt%) are Ti, Al, Pb, Sn, Nb, B, As, Zn, Bi, Zr and Ca. The main mechanical characteristics in as-received state of the material are shown in Table 2.

Table 1 *Chemical composition (in wt%) of the used AISI 304 stainless steel*

Fe	C	Si	Mn	P	S	Cr
69.51	0.023	0.271	1.600	0.047	0.034	19.19
Ni	**Mo**	**Cu**	**Co**	**V**	**W**	**other**
7.98	0.243	0.637	0.161	0.060	0.041	Balance

Table 2 *Main mechanical characteristics of the tested AISI 304 stainless steel (as-received)*

Yield limit, MPa	***Tensile strength, MPa***	***Elongation, %***	***Hardness, HB***
338^{+9}_{-18}	733^{+12}_{-10}	$44.7^{+0.3}_{-0.2}$	$250^{\pm 8}$

3.2. Experimental design

The governing factors were burnishing force F_b, feed rate f, and burnishing velocity v illustrated in Fig. 1a. The governing factor magnitudes (Table 1) were selected based on the results obtained in [20], where the authors have used one-factor-at-a-time method. The radius of the spherical-ended diamond insert was maintained at a constant value of 2 mm; according to [20] this radius magnitude provides the highest microhardness. The upper burnishing force level is 500 N, as higher values worsen the resulting roughness [20].

The transformation from physical (natural) $\tilde{x}_i$ to encoded (dimensionless) x_i variables is performed using the formula:

$$x_i = \frac{\left(\tilde{x}_i - \tilde{x}_{i,0}\right)}{\left(\tilde{x}_{i,max} - \tilde{x}_{i,0}\right)}, \quad (1)$$

where $\tilde{x}_{i,0}$ and $\tilde{x}_{i,max}$ are the average and maximum value of the physical variable, respectively.

The inverse transformation $x_i \to \tilde{x}_i$ is obtained from the formula:

$$\tilde{x}_i = \left(\tilde{x}_{i,max} - \tilde{x}_{i,0}\right)x_i + \tilde{x}_{i,0}. \quad (2)$$

The objective function was the surface microhardness Y_{HV}.

A planned experiment and a second-order optimal compositional design were used (Table 4).

3.3. Experimental results

The obtained experimental results are shown in Table 4. The average values of Ra roughness parameter and surface microhardness after turning and before DR were $Ra^{init} = 0.529\ \mu m$ and 421 HV, respectively.

Regression analysis was conducted using QStatLab software [32]. Given the chosen experimental design, the approximating polynomials are of the order no higher than the second:

$$Y_{HV}\left(\{X\}\right) = b_0 + \sum_{i=1}^{3} b_i x_i + \sum_{i=1}^{2}\sum_{j=i-1}^{3} b_{ij} x_i x_j + \sum_{i=1}^{3} b_{ii} x_i^2, \quad (3)$$

where $\{X\}$ is the vector of the governing factors $x_i, i = 1, 2, 3$.

Table 3 *Governing factors and their levels*

Governing factors	***Levels***							
	Natural, $\tilde{x}_i$				***Coded,*** x_i			
Burnishing force F_b *[N]*	$\tilde{x}_1$	*100*	*300*	*500*	x_1	*-1*	*0*	*1*
Feed rate f *[mm / rev]*	$\tilde{x}_2$	*0.02*	*0.05*	*0.08*	x_2	*-1*	*0*	*1*
Burnishing velocity v [m/min]	$\tilde{x}_3$	*50*	*85*	*120*	x_3	*-1*	*0*	*1*

Table 4 *Experimental plan and results*

№	x_1	x_2	x_3	***Microhardness HV0.05***		
				Exper.	Y_{HV} ***model***	***Model error, %***
1	*-1*	*-1*	*-1*	*595*	*597.2*	*0.370*
2	*1*	*-1*	*-1*	*658*	*653.3*	*–0.714*
3	*-1*	*1*	*-1*	*523*	*521.6*	*–0.268*
4	*1*	*1*	*-1*	*590*	*594.7*	*0.797*
5	*-1*	*-1*	*1*	*554*	*549.3*	*–0.848*
6	*1*	*-1*	*1*	*590*	*591.4*	*0.237*
7	*-1*	*1*	*1*	*488*	*492.7*	*0.207*
8	*1*	*1*	*1*	*554*	*551.8*	*–0.397*
9	*-1*	*0*	*0*	*534*	*533.2*	*–0.150*
10	*1*	*0*	*0*	*590*	*590.8*	*0.136*
11	*0*	*-1*	*0*	*585*	*590.8*	*0.991*
12	*0*	*1*	*0*	*539*	*533.2*	*–1.076*
13	*0*	*0*	*-1*	*598*	*597.2*	*–0.134*
14	*0*	*0*	*1*	*551*	*551.8*	*0.145*

Table 5 *Regression coefficients*

b_{ij}	b_0	b_1	b_2	b_3	b_{11}	b_{22}	b_{33}	b_{12}	b_{23}	b_{13}
Y_{HV}	*564.75*	*28.8*	*–28.8*	*–22.7*	*–2.75*	*–2.75*	*9.75*	*4.25*	*4.75*	*–3.5*

The polynomial coefficients of the Y_{HV} model are shown in Table 5. The model-predicted microhardness values at the experimental points are listed in Table 4. The comparison with the experimental results shows good agreement between the model and the experiment. With the exception of experimental point 12, where the error is – 1.076%, at all other experimental points the error is below 1%.

The dimensionless absolute values of the coefficients $b_i, i = 1, 2, 3,$ indicate the significance of the corresponding governing factor. The larger this value, the stronger the influence of the corresponding governing factor. The effects of burnishing force and feed rate on the microhardness are equivalent: $b_1 = \left|b_2\right| = 28.8$. The influence of burnishing velocity on the microhardness is

weaker $\left(\left|b_3\right| = 22.7\right)$, but comparable to that of the first two governing factors. In addition, the absolute value of b_{33} is the largest, compared to b_{11} and b_{22}. The analysis of variance (ANOVA) using QStatLab confirms the conclusions drawn about the significance of the governing factors (Fig. 2). It is clearly seen that when burnishing force is maintained at an upper level, and the other two factors (feed rate and burnishing velocity) occupy a lower level, the microhardness is maximal.

A graphical visualization of the microhardness model is shown in Fig. 3. Visual inspection of the surfaces confirms the conclusions drawn about the significance of the governing factors.

After substituting (1) into (3), the dependences of the microhardness on the physical governing factors are obtained. Figures 4, 5 and 6 show sections of the microhardness hypersurface (the objective function) with characteristic hyperplanes. These sections visualize the dependence of the microhardness on the corresponding governing factor.

With increasing burnishing force, the microhardness increases (Fig. 4), but at a different rate, depending on the combination of the magnitudes of the two governing factors, which maintain constant values. This result confirms the observations made in [20, 33]. With increasing burnishing force, the equivalent plastic deformation at the points of the surface layer increases, which leads to increased strain hardening. As a result, the surface microhardness increases. However, an excessive increase in burnishing force leads to a deterioration of the smoothing effect due to the introduction of surface defects [20].

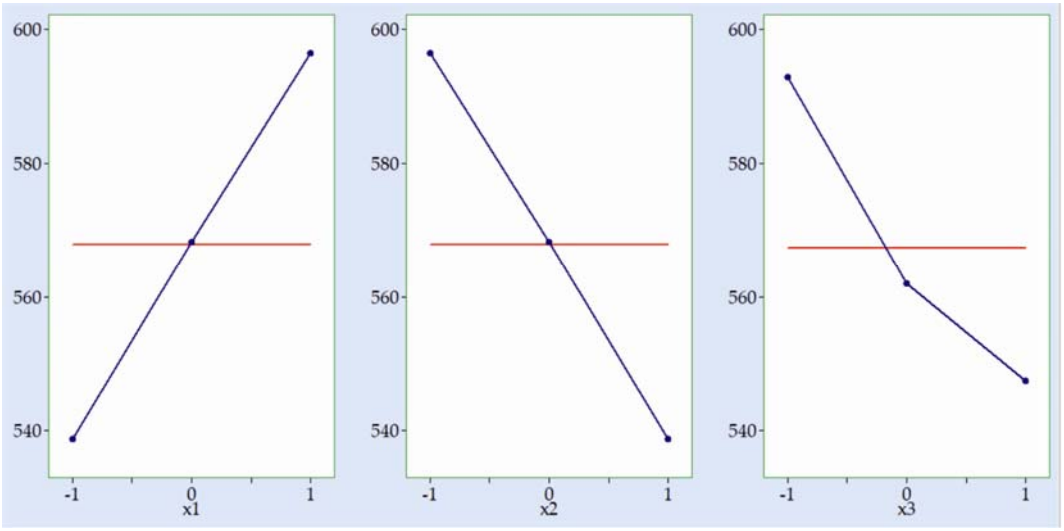

Fig. 2. ANOVA outcomes: main effects for the HV0.05 model

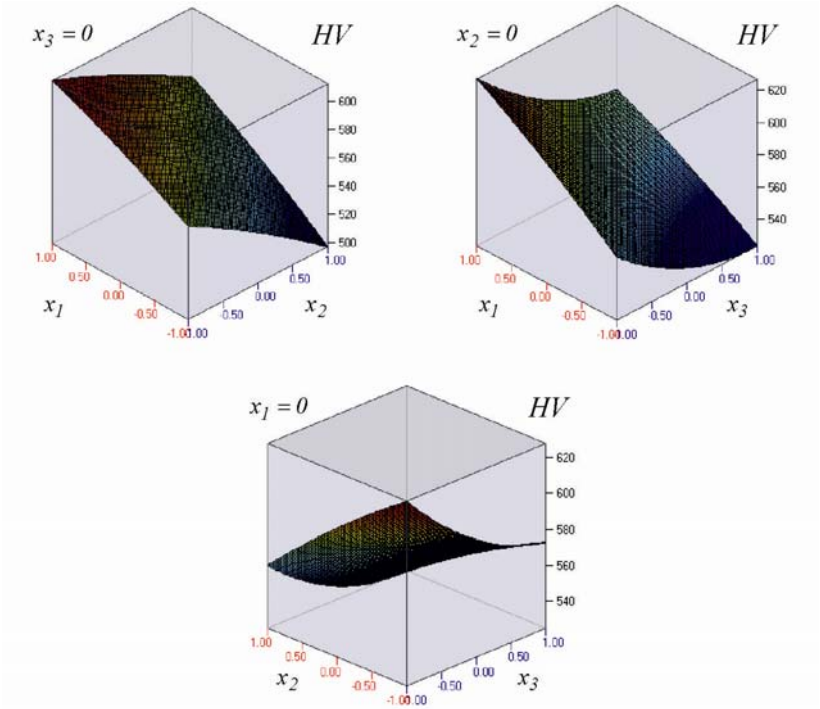

Fig. 3. Graphical visualization of the microhardness model

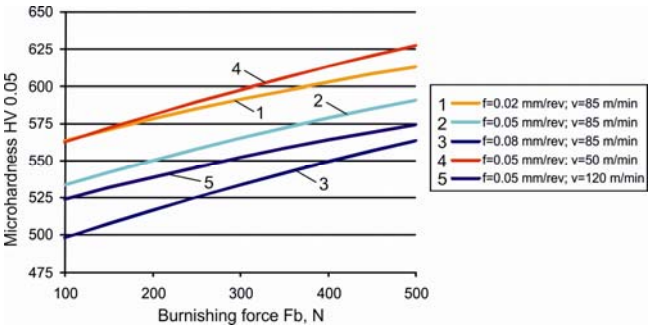

Fig. 4. Dependence of microhardness on burnishing force

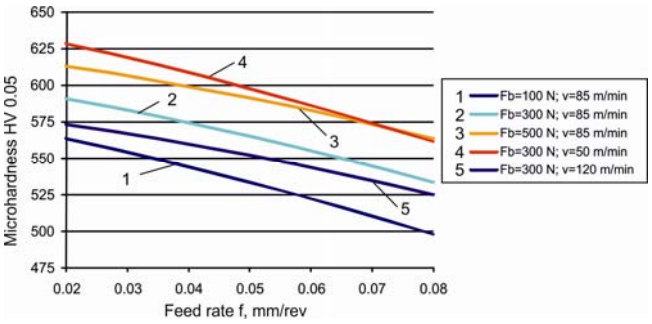

Fig. 5. Dependence of microhardness on feed rate

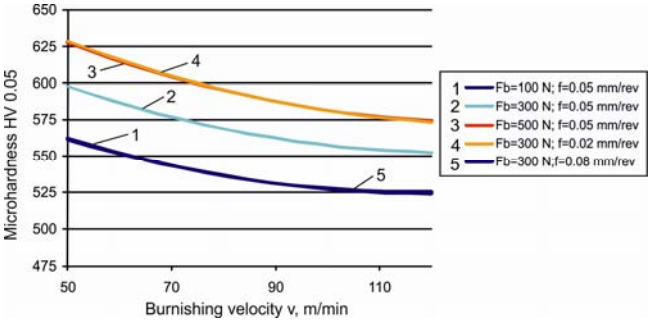

Fig. 6. Dependence of microhardness on burnishing velocity

With increasing feed rate the surface microhardness decreases at a slightly increasing rate (Fig. 5). During the DB, each point of the machined surface is subjected to cyclic loading [34, 35]. A quantitative measure of the cyclicity of the loading is the so-called cyclic loading coefficient, which increases with decreasing feed rate. As a result, a greater degree of equivalent plastic deformation accumulates, leading to an increase in the strain hardening effect, and hence to an increase in microhardness.

With increasing burnishing velocity, the microhardness decreases, but at a decreasing rate (Fig. 6). Higher burnishing velocity increases the power of the frictional forces, and thence the heat generated increases [17], causing the so-called softening effect [34]. At the same time, higher burnishing velocity leads to a higher rate of deformation. It is known that with increasing deformation rate, the yield limit of both materials approaches the tensile strength. In terms of DB, this means that the equivalent plastic deformation of the surface layer decreases, and thence the surface microhardness decreases. The obtained results confirm the observations made in [31] regarding the DB of AISI 316Ti chromium-nickel stainless steel.

4. CONCLUSIONS

A comprehensive study of the effects of the governing factors of DB of AISI 304 steel specimens on the surface microhardness obtained was conducted. As a result of this work, the major new findings (valid for the steel used and the ranges of variation of the governing factors) concerning the nature of DB process were:

- Mathematical model of the surface microhardness depending on the burnishing force, feed rate and burnishing velocity was obtained via regression analysis.
- The surface microhardness increases with increasing burnishing force due to the increased equivalent plastic deformation of the surface layer.
- With decreasing the feed rate, the surface microhardness increases due to an increase in the cyclic loading coefficient, which is a qualitative measure of the accumulation of equivalent plastic deformation in the surface layer.
- With increasing burnishing velocity, the surface microhardness decreases due to the softening effect and the increased strain rate.

ACKNOWLEDGEMENT

This research was funded by the European Regional Development Fund under the Operational Program "Scientific Research, Innovation and Digitization for Smart Transformation 2021–2027", Project CoC "Smart Mechatronics, Eco- and Energy Saving Systems and Technologies", BG16RFPR002-1.014-0005

REFERENCES

[1] Hedayati A., Najafizadeh A., Kermanpur A., Forouzan F. The effect of cold rolling regime on microstructure and mechanical properties of AISI 304L stainless steel. J Mater Process Technol, 210 (2010) 1017–1022

[2] Kumar B.R., Singh A.K., Das S., Bhattacharya D.K. Cold rolling texture in AISI 304 stainless steel. Mater Sci Eng A 364 (2004) 132–139

[3] Borgioli F. From austenitic stainless steel to expanded austenite—S phase: Formation, characteristics and properties of an elusive metastable phase. Metals, 10 (2020) 187

[4] Hoshiyama Y., Mizobata R., Miyake H. Mechanical properties of austenitic stainless steel treated by active screen plasma nitriding. Surf Coat Technol, 307 (2016) 1041–1044

[5] Juijerm P., Altenberger I. Fatigue performance enhancement of steels using mechanical surface treatments. J Met Mater Miner 17 (2007) 59–65

[6] Nikitin I., Altenberger I. Comparison of the fatigue behaviour and residual stress stability of laser-shock peened and deep rolled austenitic stainless steel AISI 304 in the temperature range 25–600 °C. Mater Sci Eng A 465 (2007) 176–182

[7] Lin Y., Lu J., Wang L., Xu T., Xue Q. Surface nanocrystalization by surface mechanical attrition treatment and its effect on structure and properties of plasma nitrided AISI 321 stainless steel. Acta Mater 54 (2006) 5599–5605

[8] Maximov J., Duncheva G., Anchev A., Dunchev V., Argirov Y. Improvement in fatigue strength of chromium–nickel austenitic stainless steels via diamond burnishing and subsequent low-temperature gas nitriding. Applied Sciences, 14 (2024) 1020

[9] Maximov J., Duncheva G., Anchev A., Dunchev V. Explicit correlation between surface integrity and fatigue limit of surface cold worked chromium-nickel austenitic stainless steels. Int. J Adv Manuf Technol 133 (2024) 6041-6058

[10] Maximov J., Duncheva G., Anchev A., Dunchev V., Argirov Y., Nikolova M. Effects of heat treatment and diamond

burnishing on fatigue behaviour and corrosion resistance of AISI 304 austenitic stainless steel. Applied Sciences, 13 (2023) 2570

[11] Korzynski M., Slide diamond burnishing. in: Nonconventional Finishing Technologies, Ed. M. Korzynski, Polish Scientific Publishers PWN, Warsaw (2013) 9-33

[12] Roohi H., Baseri H., Mirnia M., Evaluation of optimized surface characteristics in non-rotational sliding ball burnishing, Mater Manuf Proces 39 (16) (2024) 2299-2308

[13] Maximov J., Duncheva G. Finite Element Analysis and optimization of spherical motion burnishing of low-alloy steel. Proc IMechE Part C: J Mech Eng Sci 226 (1) (2012) 161-176

[14] Maximov J., Kuzmanov T., Duncheva G., Ganev N., Spherical motion burnishing implemented on lathes. Int J Mach Tools Manuf 49 (11) (2009) 824-831

[15] Luo H., Liu J., Zhong Q. Investigation of the burnishing process with PCD tool on non-ferrous metals. Int J Adv Manuf Technol 25 (5-6) (2005) 454-459

[16] Duncheva G., Maximov J., Dunchev V. et al., Single toroidal roller burnishing of 2024-T3 Al alloy implemented as mixed burnishing process. Int J Adv Manuf Technol 111 (2020) 3559-3570

[17] Maximov J., Duncheva G., Anchev A., Dunchev V. Slide burnishing versus deep rolling – a comparative analysis. J Adv Manuf Technol 110 (2020) 1923-1939

[18] Maximov J., Duncheva G. et al., Smoothing, deep or mixed diamond burnishing of low-alloy steel components – optimization procedures. J Adv Manuf Technol 106 (2020) 1917-1929

[19] Tobola D., Kania B. Phase composition and stress state in the surface layers of burnished and gas nitrided Sverker 21 and Vanadis 6 tool steels. Surf Coat Technol 353 (2018) 105-115

[20] Maximov J., Duncheva G. et al. Effect of diamond burnishing on fatigue behaviour of AISI 304 chromium-nickel austenitic stainless steel. Materials 15 (14) (2022) 4768

[21] Korzynski M., Dudek K., Kruczek B., Kocurek P., Equilibrium surface texture of valve stems and burnishing method to obtain it. Tribol Int, 124 (2018) 195-199

[22] Toboła D., Morgiel J., Maj L., TEM analysis of surface layer of Ti-6Al-4V ELI alloy after slide burnishing and low-temperature gas nitriding. Appl Surf Sci 515 (2020) 145942

[23] Maximov J., Anchev A., Duncheva G. et al., Impact of slide diamond burnishing additional parameters on fatigue behaviour of 2024-T3 Al alloy. Fatigue Fract Eng Mater Struct 42 (1) (2019) 363-373

[24] Maximov J., Anchev A., Dunchev V. et al. Effect of slide burnishing basic parameters on fatigue performance of 2024-T3 high-strength aluminium alloy. Fatigue Fract Eng Mater Struct 40 (11) (2017) 1893-1904

[25] Duncheva G., Maximov J. et al., Enhancement of the wear resistance of CuAl9Fe4 sliding bearing bushings via diamond burnishing. Wear 510-511 (2022) 204491

[26] Duncheva G., Maximov J. et al., Multi-objective optimization of internal diamond burnishing process. Mater Manuf Process 37 (4) (2022) 428-436

[27] Duncheva G., Maximov J. et al., Improvement in wear resistance performance of CuAl8Fe3 single-phase aluminum bronze via diamond burnishing. J Mater Eng Perform (31) (2022) 2466-2478

[28] Varga G., Ferencsik V., Experimental examination of surface micro-hardness improvement ratio in burnishing of external cylindrical workpieces. Cutting & Tools in Technological System 93 (2020) 114-121

[29] Okada M., Shinya M., Matsubara H. et al., Development and characterization of diamond tip burnishing with a rotary tool. J Mater ProcessTechnol Vol. 244, 2017, 106-115.

[30] Skoczylas A., Zaleski K., Matuszal J. et al., Influence of slide burnishing parameters on the surface layer properties of stainless steel and mean positron lifetime. Materials, 15 (2022) 8131

[31] Maximov J., Duncheva G. et al. Effect of slide burnishing method on the surface integrity of AISI 316Ti chromium-nickel steel. J Braz Soc Mech Sci Eng 40 (2018) 194

[32] Vuchkov I.N., Vuchkov I.I., QStatLab Professional, version 6.1.1.3; Statistical Quality Control Software, User's Manual; QStatLab: Sofia, Bulgaria (2009)

[33] Kuznetsov V., Makarov A., Skorobogatov A., Skorinina P., Luchko S., Sirosh V., Chekan N. Influence of normal force on smoothing and hardening of the surface layer of steel 03X16N15M3T1 during dry diamond smoothing with a spherical indenter. Metal Processing 24 (1) (2022) 6-22 (in Russian)

[34] Maximov J., Duncheva G., Anchev A., Ganev N., Dunchev V. Effect of cyclic hardening on fatigue performance of slide burnishing components made of low-alloy medium carbon steel. Fatigue Fract Eng Mater Struct 42 (6) (2019) 1414-1425

[35] Kuznetsov V., Smolin I., Dmitriev A., Tarasov S., Gorgots V. Toward control of subsurface strain accumulation in nanostructuring burnishing on thermostrengthened steel. Surf Coat Techol 285 (2016) 171-178